RSC Advances

PAPER

View Article Online
View Journal | View Issue

Cite this: *RSC Adv.*, 2017, **7**, 56087

Green preparation of nitrogen doped carbon quantum dot films as fluorescent probes

Yanfei He,[a] Lina Liang,[a] Qinghao Liu,*[a] Jinchun Guo,[b] Dong Liang[a] and Hongyan Liu[c]

Received 14th October 2017
Accepted 6th December 2017

DOI: 10.1039/c7ra11332c

rsc.li/rsc-advances

To prepare nitrogen doped carbon dots (NCDs) with excellent luminescence efficiency, a facile hydrothermal method was developed using cabbage juice as the carbon source and poly ethylene polyamine (PP) as the nitrogen source. Then, as-prepared NCDs were grafted onto calcium alginate to produce calcium alginate film (CA-NCDs), and the CA-NCDs were used as a fluorescent probe. The significant quenching effect of Fe^{3+} was established. The ratio of fluorescence intensity (F/F_0) of the CA-NCDs had a linear relationship with the concentration of Fe^{3+} within the range of 0 to 48 μM (R^2 was 0.9947) and the detection limit was 1.4 nM. In addition, the recovery of spiked samples ranged from 98.6% to 103.1%. Most importantly, the amino-functionalized CA-NCD fluorescent probe can be successfully applied for the detection of trace Fe^{3+} in water samples.

The ferric ion (Fe^{3+}) is one of the most essential metal ions in immune systems, playing a significant role in many pathological and physiological processes including oxidation reactions, cellular metabolism, electron transfer, as well as RNA and DNA synthesis.[1–3] Therefore, it is significant to establish effective analytical methods for highly sensitive and selective detection of Fe^{3+} in aqueous solutions.[4] Recently, a variety of detection methods, such as atomic absorption/emission spectroscopy, atomic fluorescence spectrometry (CV-AAS),[5–7] and inductive coupled plasma atomic emission spectroscopy (ICP-MS),[8–10] have been developed to measure the level of Fe^{3+}. However, most of these methods usually suffered from expensive instrumentation, complicated operation and the use of toxic and expensive reagents, which limited their practical applications in the routine monitoring of Fe^{3+}.[11,12] It is necessary to develop an economical, simple, and green strategy to synthesize optical probes. Thanks to its ease of operation, fast response and high efficiency, the fluorescent probe has been one of the most feasible and promising methods to solve the aforementioned problems.[13–15]

Carbon quantum dots (CDs) have attracted much attention due to their unique properties,[16–21] including high quantum yield,[22] low cost, low toxicity, good biocompatibility,[23] good dispersibility in aqueous solution,[24] ease of functionalization,[25] *etc.* Meanwhile, CDs have been applied in various fields such as bioimaging,[26,27] medical diagnosis, analytical chemistry,[28] *etc.* However, the fluorescence quantum yield of CDs is relatively low.[29,30] But recently, some research reported that the fluorescence properties of CDs were improved by doping nitrogen into the carbon nanoparticles.[31,32] The reason is probably that the large conjugated carbon structure of CDs is broken and the surface defects of CDs was passivated.[33] Furthermore, CDs in aqueous solution are not easy to recycle.

Herein, green NCDs have been synthesized with cabbage juice as the carbon source and polyethylene polyamine as the nitrogen source. Moreover, the as-prepared NCDs were grafted onto calcium alginate and a calcium alginate thin film was obtained. Due to the fluorescence quenching effect of Fe^{3+} on CA-NCDs, CA-NCDs were used as a fluorescent probe and applied to the Fe^{3+} detection.

1 Experimental

1.1 Chemicals and instruments

Cabbage was purchased from the local market. Poly ethylene polyamine (PP), $HgCl_2$, $AlCl_3$, $CuCl_2$, $CaCl_2$, $FeCl_3$, NaCl, $MgCl_2$, AgCl, KNO_3, $MnSO_4 \cdot H_2O$, $Zn(NO_3)_2$, $Ba(NO_3)_2$, $Zn(NO_3)_2$ and $Ni(NO_3)_2$ were purchased from Tianjin Chemical Reagent Co. All reagents were of analytic grade and used as received without any further purification. Doubly distilled water was used in all experiments. Tap water samples were collected from our laboratory, and lake water samples were obtained from the Fen River in Taiyuan City, Shanxi Province, China. All water samples were used without any further pretreatment.

All fluorescence measurements were performed using a Cary Eclipse fluorescence spectrophotometer (Varian, American), Fourier transform infrared (FTIR) spectra were recorded on

[a]School of Chemical Engineering and Technology, North University of China, Taiyuan 030051, Shanxi Province, People's Republic of China. E-mail: liuqinghao@nuc.edu.cn
[b]School of Environmental and Safety Engineering, North University of China, Taiyuan 030051, Shanxi Province, People's Republic of China
[c]Institute of Plant Protection, Henan Academy of Agricultural Sciences, Zhengzhou 450002, Henan Province, People's Republic of China

a Fourier-transform infrared spectrometer (8400S, Daojin, Japan). Absorption spectra were recorded using a UV-vis double-beam spectrometer (UV-2450, Purkinje Daojin, Japan).

1.2 Synthesis of NCDs

35 mL cabbage juice were transferred into a 100 mL stainless-steel teflon lined vessel and heated at 200 °C for 5 h. After the reaction, the reactor was cooled down to room temperature. Then, poly ethylene polyamine was added, and the solution was hydrothermally treated again at 200 °C for another 5 h. Transparent brown-yellow solution was gained after the reactors cooled down to room temperature. The product was centrifuged at a high speed (12 000 rpm) for 10 min to remove the large particles, and then the solution was dialyzed in a dialysis bag for 3 d ($M_w = 3000$). Eventually, pure NCDs were obtained by rotary evaporation.

1.3 Preparation of CA-NCDs

1.8 g calcium alginate was dissolved in 10 mL NCDs and 50 mL deionized water, the mixture solution was magnetic stirred for 4 h. Then, the solution was statically defoamed. The sodium alginate sol was poured into the culture dish by tape casting. A dense crosslinked calcium alginate film (CA-NCDs) was formed by spraying 1.5 mol L^{-1} $CaCl_2$ solution to the surface of sodium alginate sol, and then vacuum dried at 50 °C to constant weight.

1.4 Fluorescence detection of Fe^{3+} by CA-NCDs

CA-NCDs was added into 3 mL of Fe^{3+} solution, followed by adding Fe^{3+} ions solution with different concentrations (0, 4, 8, 12, 16, 20, 24, 28, 32, 36, 40, 44, 48 μM), then filtered and dried at 50 °C under vacuum. All samples were incubated for 30 min at room temperature and recorded the fluorescence spectra at the excitation wavelength of 350 nm. The used films were immersed in ethylenediaminetetraacetic acid (EDTA) solution for 5 min, rinsed repeatedly with deionized water, and vacuum dried to constant weight. They were used for repeated examinations of Fe^{3+} ions.

2 Results and discussion

2.1 Optical properties of the CA-NCDs

The UV-vis absorption and fluorescence spectra of CA-NCDs were studied and shown in Fig. 1. As shown in Fig. 1A, the UV-vis absorption spectrum of CA-NCDs show a broad absorption band with a strong peak at 350 nm, which could be ascribed to the n–π* transition of the C=O bond and π–π* transition of C=C.[34,35] The peak at 350 nm is due to the trapping of excited state energy on the CA-NCDs surfaces.[36–38] The CA-NCDs are yellow color under daylight (Fig. 1A-a) and emits a bright blue fluorescence under the illumination of 365 nm UV light (Fig. 1A-b). The fluorescent quantum yield of CA-NCDs is about 53.3% using quinine sulfate (QY 54% in 0.1 mol L^{-1} H_2SO_4, $\lambda_{ex} = 360$ nm) as the reference.

As shown in Fig. 1B, the fluorescence spectra of CA-NCDs reveal that the maximum excitation wavelength is at 350 nm, and exhibit a narrow and symmetrical emission peak which appear at 469 nm. The significantly increase of fluorescence intensity of CA-NCDs might be attribute to the defects on CA-NCDs surface and the passivation of functional groups.[36,38]

As shown in Fig. 1C, the fluorescence intensity increases initially till 350 nm and then decreases gradually with increasing excitation wavelength, indicating an excitation-dependent emission. Such a behavior can be explained by the different sizes of CA-NCDs and the distribution of different surface states. The excitation wavelength is at 350 nm and the strongest emission is at 469 nm, which is consistent to most reports of CA-NCDs.[39,40]

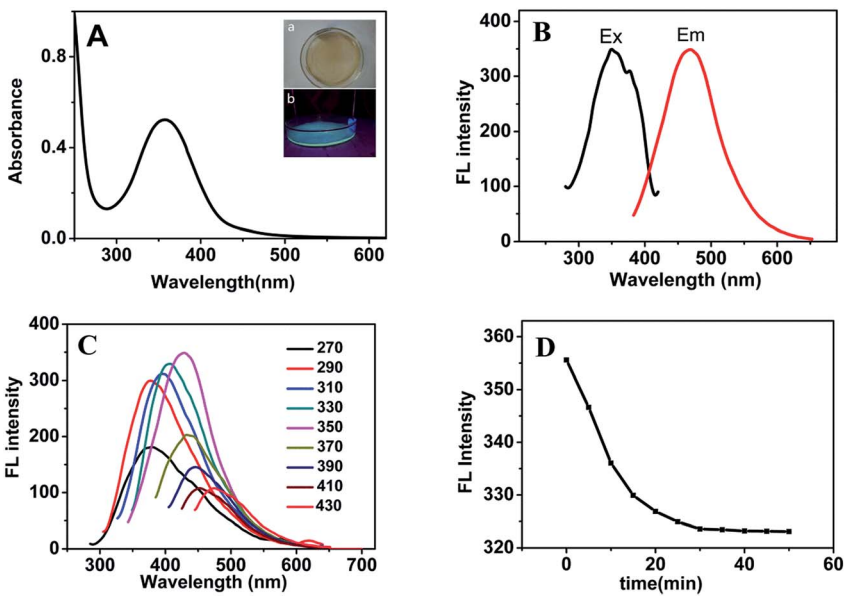

Fig. 1 (A) UV/vis absorption of the CA-NCDs, inset shows the colors of CA-NCDs under visible light (a) and UV light (b), (B) fluorescence excitation and emission spectra of the CA-NCDs, (C) emission spectra of the CA-NCDs at different excitation wavelengths from 300 to 390 nm in 20 nm increments, (D) the fluorescence intensity of CA-NCDs varying with time.

Fig. 1D shows the fluorescence intensity of CA-NCDs varying with time. At a given time, the fluorescence intensity decreases constantly with time. However, when the incubation time is above 30 min, the decrease of the fluorescence intensity with time becomes insignificant. Also, the fluorescence intensity at 30 min is very close to that at 50 min. Therefore, 30 min was identified as the optimal incubation time.

2.2 Characterization of the CA-NCDs

The morphology of CA-NCDs was characterized by transmission electron microscopy (TEM). As shown in Fig. 2A, these CA-NCDs are mostly spherical shape that are uniform, highly monodisperse and no aggregation emerged, with an average diameter of about 1.8 nm.

Fig. 2B shows FTIR spectra of NCDs and CA-NCDs. For NCDs (Fig. 2B-a), the peak at 3455 cm^{-1} is correspond to the stretching vibrations of O–H and N–H, which reveals that the amino and hydroxy groups of NCDs, and demonstrate the good water-solubility of NCDs. The FTIR spectrum also exhibits stretching vibration absorption band of C–H at 2923 cm^{-1}.[41,42] Furthermore, peaks at 1712 cm^{-1}, 1397 cm^{-1}, 1184 cm^{-1} and 1500 cm^{-1} are originated from C=O, N–H, C–N and C–O, respectively suggesting that NCDs have been successfully obtained. For CA-NCDs (Fig. 2B-b), the absorption peak at 3439 cm^{-1} is similar to those of the carbon dots. In comparison with Fig. 2B-a, the peaks at 1098 cm^{-1} come from the stretching vibrations of C–O in calcium alginate molecule. The C–O–Ca–O–Ca group is formed due to the cross-linking of calcium ions, so the stretching vibration absorption of C–O is enhanced. The peaks around 1633 cm^{-1} and 1410 cm^{-1} are attributed to the symmetric stretching vibration and asymmetric stretching vibration of C–H, respectively. Peak at 786 cm^{-1} corresponds to the stretching vibration of C–C in calcium alginate molecule.

2.3 Selectivity of the CA-NCDs for Fe^{3+} detection

To evaluate the selectivity and specificity of CA-NCDs as a fluorescent probe for Fe^{3+} detection, the fluorescence responses of CA-NCDs were investigated in the presence of different metal ions under same concentrations, including Hg^{2+}, Cu^{2+}, Pb^{2+}, Mg^{2+}, Al^{3+}, K^{+}, Na^{+}, Ni^{2+}, Zn^{2+}, Ba^{2+}, Fe^{3+}, Ca^{2+}, Mn^{2+} and Ag^{+}. As shown in Fig. 3A, a strong fluorescence quenching is observed in the presence of Fe^{3+}, while other metal ions show only a slight quenching effect on the fluorescence of CA-NCDs. This may be because the formed CA-NCDs-Fe^{3+} complexes would facilitate non-radiative electron/hole recombination annihilation through an effective electron transfer process, leading to the distinguished fluorescence quenching effects.[42,43] The results indicate that the obtained CA-NCDs possess excellent selectivity towards Fe^{3+} and can serve as fluorescence probe for Fe^{3+} detecting.

Fig. 3B shows the interference tests, it is seen that the fluorescence intensity of CA-NCDs remains almost unchanged after mixing with any one of the interference metal ions. However, the significant fluorescence quench is observed on further addition of Fe^{3+} even in the presence of each interfering metal ion, while the other metal ions shows only a slight quenching effect. The results indicate that these metal ions do not interfere

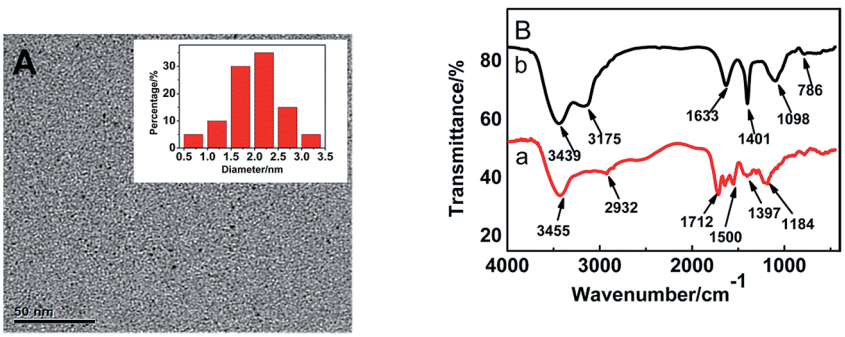

Fig. 2 (A) TEM image of the CA-NCDs. Inset shows the distribution of particle sizes (B) FTIR spectrum of NCDs (a) and CA-NCDs (b).

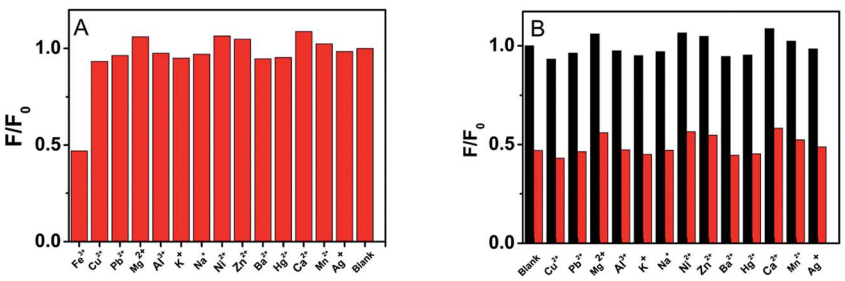

Fig. 3 (A) Selectivity of ions as using CA-NCDs probes. The concentration of all the metal ions is 25 μM (F_0 and F correspond to the fluorescence intensities of CA-NCDs in the absence and presence of metal ions), (B) the fluorescence intensities of M and CA-NCDs (M represents any one of the metal ions except for Fe^{3+}) solutions before (blank) and after (red) mixing with Fe^{3+}.

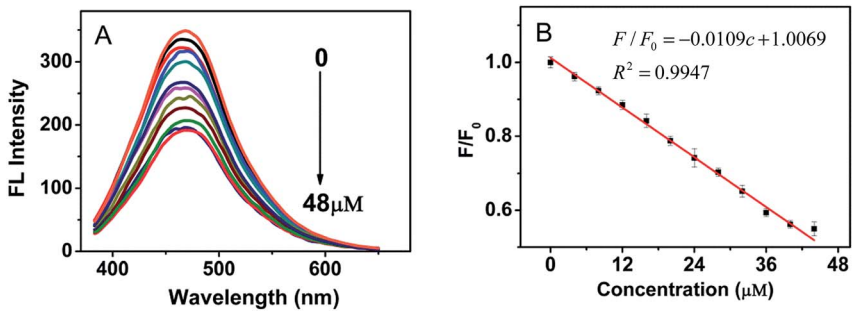

Fig. 4 (A) Fluorescence response of CA-NCDs in the presence of different concentrations of Fe^{3+} ions (from top to bottom: 0, 4, 8, 12, 16, 20, 24, 28, 32, 36, 40, 44, 48 μM), (B) the linear relationship of F/F_0 *versus* the concentration of Fe^{3+} ions.

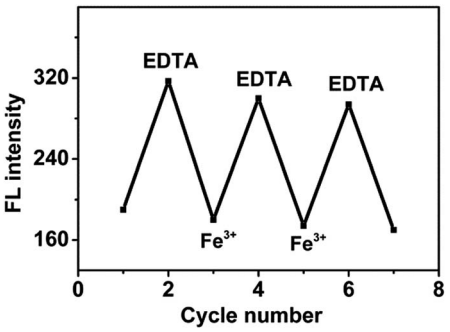

Fig. 5 Fluorescence intensity change for the hydrogel films after alternate treatment with an aqueous solution of Fe^{3+} (2×10^{-5} mol L^{-1}) and EDTA (2×10^{-4} mol L^{-1}).

with the detection of Fe^{3+}. Since Fe^{3+} ions have strong affinity toward hydroxyl, carboxyl and amino groups of CA-NCDs than the other metal ions to form stable chelate complexes, it is reasonable to observe the outstanding selectivity and specificity of CA-NCDs to Fe^{3+}. This suggests that the obtained CA-NCDs have high selectivity towards Fe^{3+} ions.

2.4 Fluorescence detection of Fe^{3+} using CA-NCDs

To further explore the interaction between Fe^{3+} and CA-NCDs. A series of Fe^{3+} ions solutions with the concentration range from 0 to 48 μM were added into the CA-NCDs with a fixed concentration. The fluorescence emission spectra was excited at the wavelength of 350 nm. As shown in Fig. 4A, the fluorescent intensity of CA-NCDs is gradually decreased with increasing the concentration of Fe^{3+}. This is presumably due to the binding of Fe^{3+} on CA-NCDs surface accelerates the non-radiative recombination of the excitons through an effective electron transfer process,[44] leading to a substantial decrease of the fluorescence of CA-NCDs.[43] Fig. 4B clearly shows the linear relationship between fluorescence intensities and Fe^{3+} concentration, the calibration curve can be expressed as $F/F_0 = 1.0069 - 0.0109c$ with correlation coefficient (R^2) of 0.9947 (F_0 and F are the fluorescent intensities of the CA-NCDs without and with added Fe^{3+}, respectively). The detection limit ($3\sigma/s$) for Fe^{3+} is 1.4 nM, where σ is the standard deviation of ten blank measurements, and s is the slope of the calibration curve, which is comparable or even better than those reported parameters in the literature.

2.5 Repeatability study of Fe^{3+} detection

The fluorescence of CA-NCDs was quenched when Fe^{3+} was added, and recovered when the treated CA-NCDs were immersed in EDTA solution. As shown in Fig. 5, no. 1, 3, 5 and 7 are fluorescence intensity of CA-NCDs treated with Fe^{3+} ions solutions, and no. 2, 4 and 6 are that after recovered with EDTA solution. The results show that the fluorescence intensity of CA-NCDs changed regularly, leading to reproducible changes in fluorescence intensity over three cycles. Thus, the CA-NCDs could be serving as a reusable fluorescent probe for Fe^{3+} detection in water samples.

2.6 Fe^{3+} measurement in real water samples

To test the feasibility in real water samples, the CA-NCDs was further used to quantify the Fe^{3+} in mineral water, tap water and Fen River water by using UV-vis sensor. Fen River water was obtained from the Fen River water Taiyuan, Shanxi province, China. Wahaha mineral water was purchased from the local market. Tap water was obtained from the laboratory. The water samples were first filtered with medium speed filter paper, and then centrifuged at 12 000 rpm for 10 min to remove the large suspended particles. The relative standard deviation values of Fe^{3+} and the recoveries were obtained. As shown in Table 1, the

Table 1 Determination results of Fe^{3+} in water samples

Samples	Found (μM)	RSD (%) ($n = 6$)	Added (μM)	Total found (μM)	Recover (%) ($n = 6$)
Mineral water	0.362	1.26	0.5	0.855	98.6%
Tap water	0.380	1.98	0.5	0.886	101.2%
Fen River water	0.573	2.03	0.7	1.295	103.1%

result demonstrated that the recovery is ranged from 98.6% to 103.1%. The results also show that the prepared CA-NCDs may be a potential sensing platform for the detection of Fe^{3+} in real water samples.

3 Conclusions

In this work, a green, facile and low toxicity hydrothermal method has been developed and used for the preparation of water-soluble fluorescent N-doped carbon quantum dots. The obtained NCDs were grafted onto calcium alginate to form CA-NCDs. The CA-NCDs show a high fluorescence intensity and excitation-dependent emission behavior. Meanwhile, the CA-NCDs emitted strong blue fluorescence and their fluorescence can be quenched by Fe^{3+}. There is a good linear relationship between the Fe^{3+} concentrations within 0–48 μM and the fluorescence quenching rates of CA-NCDs. Furthermore, the interaction of Fe^{3+} ions with CA-NCDs can be observed through the fluorescence quenching effect with EDTA. The CA-NCDs have good hydrophilic properties for ion detection in water and a higher recovery rate in practical water application.

Conflicts of interest

There are no conflicts to declare.

Acknowledgements

This work was supported by the National Natural Science Foundation of China (No. 21406211) and the Natural Science Foundation of Shanxi (No. 201701D221196).

References

1 R. L. Liu, D. Q. Wu, S. H. Liu, K. Koynov, W. Knoll and Q. Li, *Angew. Chem.*, 2009, **48**, 4598–4601.
2 G. Sivaraman, V. Sathiyaraja and D. Chellappa, *J. Lumin.*, 2014, **145**, 480–485.
3 E. M. Nolan and S. J. Lippard, *J. Mater. Chem.*, 2005, **15**, 2778–2783.
4 Z. Yan, J. Shu, Y. Yu, Z. Zhang, Z. Liu and J. Chen, *Luminescence*, 2015, **30**, 388–392.
5 X. J. Gong, W. J. Lu, M. C. Paau, Q. Hu, X. Wu, S. M. Shuang, C. Dong and M. M. Choi, *Anal. Chim. Acta*, 2015, **861**, 74–84.
6 Z. Li, Y. Ni and S. Kokot, *Biosens. Bioelectron.*, 2015, **74**, 91–97.
7 M. Ghaedi, M. R. Fathi, A. Shokrollahi and F. Shajarat, *Anal. Lett.*, 2006, **39**, 1171–1185.
8 L. Fang, C. Zhao, Y. Chen, L. M. Sheng, K. An, L. M. Yu, W. Ren and X. L. Zhao, *Carbon*, 2015, **91**, 408–415.
9 X. Y. Jia, Y. Han, X. L. Liu, T. C. Duan and H. T. Chen, *Spectrochim. Acta, Part B*, 2011, **66**, 88–92.
10 Y. J. Gong, X. B. Zhang, Z. Chen, Y. Yuan, Z. Jin, L. Mei, J. Zhang, W. Tan, G. L. Shen and R. Q. Yu, *Analyst*, 2012, **137**, 932–938.
11 L. Cao, X. Wang, M. J. Meziani, F. S. Lu, H. F. Wang, P. G. Luo, Y. Lin, B. A. Harruff, L. M. Veca, D. Murray, S.-Y. Xie and Y.-P. Sun, *J. Am. Chem. Soc.*, 2007, **129**, 11318–11319.
12 V. Roy, M. Amyot and R. Carignan, *Environ. Sci. Technol.*, 2009, **43**, 5605–5611.
13 F. X. Wang, Z. Y. Gu, W. Lei, W. J. Wang, X. F. Xia and Q. L. Hao, *Sens. Actuators, B*, 2014, **190**, 516–522.
14 J. H. Kim, S. H. Han and B. H. Chung, *Biosens. Bioelectron.*, 2011, **26**, 2125–2129.
15 J. Ju and W. Chen, *Biosens. Bioelectron.*, 2014, **58**, 219.
16 R. Zhang and W. Chen, *Biosens. Bioelectron.*, 2014, **55**, 83.
17 X. H. Gao, Y. Z. Lu, R. Z. Zhang, S. J. He, J. Ju, M. M. Liu, L. Li and W. Chen, *J. Mater. Chem. C*, 2015, **3**, 2302.
18 W. Chen and A. Chem, *Anal. Chem.*, 2015, **87**, 1903.
19 J. Ju, R. Zhang and W. Chen, *Sens. Actuators, B*, 2016, **228**, 66–73.
20 J. Ju, R. Z. Zhang, S. J. He and W. Chen, *RSC Adv.*, 2014, **4**, 52583–52589.
21 X. H. Gao, C. Du, Z. H. Zhuang and W. Chen, *J. Mater. Chem. C*, 2016, **4**, 6927.
22 S. N. Baker and G. A. Baker, *Angew. Chem., Int. Ed. Engl.*, 2010, **49**, 6726–6744.
23 Y. Xu, M. Wu, Y. Liu, X. Z. Feng, X. B. Yin, X. W. He and Y. K. Zhang, *Chem.–Eur. J.*, 2013, **7**, 2276–2283.
24 J. J. Huang, Z. F. Zhong, M. Z. Rong, X. Zhou, X. D. Chen and M. Q. Zhang, *Carbon*, 2014, **70**, 190–198.
25 F. Y. Yan, Y. Zou, M. Wang, X. L. Mu, N. Yang and L. Chen, *Sens. Actuators, B*, 2014, **192**, 488–495.
26 J. Y. Hou, J. Dong, H. S. Zhu, X. Teng, S. Y. Ai and M. L. Mang, *Biosens. Bioelectron.*, 2015, **68**, 20–26.
27 Y. Zou, F. Y. Yan, T. C. Zheng, D. C. Shi, F. Z. Sun, N. Yang and L. Chen, *Talanta*, 2015, **135**, 145–148.
28 G. Q. Xiang, L. L. Li, X. M. Jiang, L. J. He and L. Fan, *Anal. Lett.*, 2013, **4**, 706–716.
29 T. Ueno and T. Nagano, *Nat. Methods*, 2011, **8**, 642–645.
30 Y. S. Xia and C. Q. Zhu, *Talanta*, 2008, **1**, 215–221.
31 S. Y. Lim, W. Shen and Z. Gao, *Chem. Soc. Rev.*, 2015, **44**, 362–381.
32 S. Barman and M. Sadhukhan, *J. Mater. Chem.*, 2012, **22**, 21832–21837.
33 C. Zhu, J. Zhai and S. Dong, *Chem. Commun.*, 2012, **48**, 9367–9369.
34 J. I. Paredes, S. Villar-Rodil, A. Martínez-Alonso and J. M. D. Tascón, *Langmuir*, 2008, **24**, 10560.
35 S. L. Hu, K. Y. Niu, J. Sun, J. Yang, N. Q. Zhao and X. W. Du, *J. Mater. Chem.*, 2009, **19**, 484–488.
36 P. Anilkumar, X. Wang, L. Cao, S. Sahu, J. H. Liu, P. Wang, K. Korch, K. N. Tackett, A. Parenzan and Y. P. Sun, *Nanoscale*, 2011, **5**, 2023–2027.
37 X. Wang, L. Cao, S. T. Yang, F. S. Lu, M. J. Meziani, L. L. Tian, K. W. Sun, M. A. Bloodgood and Y. P. Sun, *Angew. Chem., Int. Ed.*, 2010, **31**, 5310–5314.
38 Z. Z. Zhang, W. H. Sun and P. Y. Wu, *ACS Sustainable Chem. Eng.*, 2015, **3**, 1412–1418.
39 S. Zhu, Q. Meng, L. Wang, J. Zhang, Y. Song, H. Jin, K. Zhang, H. Sun, H. Wang and B. Yang, *Angew. Chem., Int. Ed. Engl.*, 2013, **52**, 3953–3957.
40 C. X. Wang, Z. Z. Xu, H. Cheng, H. H. Lin, M. G. Humphrey and C. Zhang, *Carbon*, 2015, **82**, 87–95.

41 J. Y. Hou, J. L. Li, J. C. Sun, S. Y. Ai and M. L. Wang, *RSC Adv.*, 2014, **70**, 37342–37348.
42 H. Huang, J. J. Lv, D. L. Zhou, N. Bao, Y. Xu, A. J. Wang and J. J. Feng, *RSC Adv.*, 2013, **44**, 21691–21696.
43 L. Zhou, Y. H. Lin, Z. Z. Huang, J. S. Ren and X. G. Qu, *Chem. Commun.*, 2012, **48**, 1147–1149.
44 Y. Hou, Q. Lu, J. Deng, H. Li and Y. Zhang, *Anal. Chim. Acta*, 2015, **866**, 69–74.